JCTC Journal of Chemical Theory and Computation

Article

pubs.acs.org/JCTC

Lennard-Jones Lattice Summation in Bilayer Simulations Has Critical Effects on Surface Tension and Lipid Properties

Christian L. Wennberg, Teemu Murtola, Berk Hess, and Erik Lindahl*

Swedish e-Science Research Center and Department of Theoretical Physics, KTH Royal Institute of Technology, Box 1031, 17121 Solna, Sweden

Center for Biomembrane Research, Department of Biophysics and Biochemistry, Stockholm University, 106 91 Stockholm, Sweden

ABSTRACT: The accuracy of electrostatic interactions in molecular dynamics advanced tremendously with the introduction of particle-mesh Ewald (PME) summation almost 20 years ago. Lattice summation electrostatics is now the de facto standard for most types of biomolecular simulations, and in particular, for lipid bilayers, it has been a critical improvement due to the large charges typically present in zwitterionic lipid headgroups. In contrast, Lennard-Jones interactions have continued to be handled with increasingly longer cutoffs, partly because few alternatives have been available despite significant difficulties in tuning cutoffs and parameters to reproduce lipid properties. Here, we present a new Lennard-Jones PME implementation applied to lipid bilayers. We confirm that long-range contributions are well approximated by dispersion corrections in simple systems such as pentadecane (which makes parameters transferable), but for inhomogeneous and anisotropic systems such as lipid bilayers there are large effects on surface tension, resulting in up to 5.5% deviations in area per lipid and order parameters—far larger than many differences for which reparameterization has been attempted. We further propose an approximation for combination rules in reciprocal space that significantly reduces the computational cost of Lennard-Jones PME and makes accurate treatment of all nonbonded interactions competitive with simulations employing long cutoffs. These results could potentially have broad impact on important applications such as membrane proteins and free energy calculations.

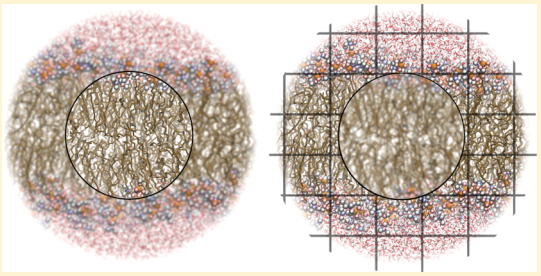

1. INTRODUCTION

The treatment of nonbonded interactions has been a bottleneck since the early days of particle-based simulations because of their high computational cost that tends to dominate the total runtime of molecular dynamics. For a periodic system some sort of cutoff has to be applied, but this can lead to severe issues for electrostatics since the classical r^{-1} form of the potential does not even converge for a general system with mobile charges, regardless of cutoff. Historically, this has been circumvented by grouping charges to obtain clusters with approximately dipolar interactions. This has made it somewhat more acceptable to truncate the interactions, but several studies in the literature have shown that this cutoff paradigm still introduces major artifacts in simulations, for instance artificial ordering.[1−6] For small periodic systems, it is possible to fully evaluate the periodic long-range component using the Ewald sum introduced already in 1921 for crystals,[7] but since the computational complexity of this method increases as $N^{3/2}$ (where N is the number of particles in the system), it was never broadly adopted for large biomolecular simulations. However, this situation changed dramatically in 1993 when Darden and co-workers, inspired by the work of Hockney and Eastwood,[8] published the fast Particle-Mesh Ewald (PME) lattice summation algorithm.[9,10] Over the last 15 years, PME has become the method of choice for treating electrostatics in biomolecular simulations. It has virtually completely removed discussions about specific cutoff artifacts, and compared to truncation schemes with large interaction radii PME can even be faster than cutoff approximations.

In contrast, the cutoff approximation has been much less debated for nonpolar van der Waals interactions where the absolute error for an interaction is considerably smaller at typical cutoffs around 10 Å. For most biomolecular force fields, this type of interaction is formulated through the Lennard-Jones (LJ) form with separate repulsion and attraction (dispersion) terms

$$U_{\mathrm{LJ}}(r_{ij}) = 4\epsilon_{ij}\left[\left(\frac{\sigma_{ij}}{r_{ij}}\right)^{12} - \left(\frac{\sigma_{ij}}{r_{ij}}\right)^{6}\right] = \frac{C_{ij}^{(12)}}{r_{ij}^{12}} - \frac{C_{ij}^{(6)}}{r_{ij}^{6}} \quad (1)$$

where r_{ij} is the interparticle distance, σ_{ij} the distance at which the potential is zero, and ϵ_{ij} describes the interaction strength. Alternatively, one can use $C_{ij}^{(12)}$ and $C_{ij}^{(6)}$ to directly describe the repulsion and dispersion components, respectively. For arbitrary particle types i and j, the specific parameters have to be derived using combination rules discussed in more detail in the theory section. In some cases, the repulsion is more accurately modeled with an exponential term, but in both cases,

Received: February 22, 2013
Published: June 21, 2013

the van der Waals interaction strength at long distances will be dominated by the dispersion term.

Although the r^{-6} term exhibits a much faster falloff than electrostatics, all these dispersion interactions are attractive (in contrast to electrostatics where the sign fluctuates), which means there will still be non-negligible effects on pressure and volume when introducing a cutoff for computational efficiency. However, the uniform sign itself makes it possible to correct for this error by approximating a correction beyond the cutoff

$$U_{\mathrm{dc}} = \frac{N}{2}\rho \int_{r_c}^{\infty} 4\varepsilon\left[\left(\frac{\sigma}{r}\right)^{12} - \left(\frac{\sigma}{r}\right)^{6}\right] g(r) 4\pi r^2 \, \mathrm{d}r \tag{2}$$

Here, N is the number of particles in the system, ρ the average density, and σ, ε the interaction parameters that we initially assume are identical for all particles. The term $g(r)$ is the pair distribution function that fluctuates for smaller distances, but after a sufficiently large cutoff, r_c, it can be approximated with unity to evaluate the integral to

$$U_{\mathrm{dc}} = 8N\pi\rho\varepsilon\sigma^3\left[\frac{1}{9}\left(\frac{\sigma}{r_c}\right)^{9} - \frac{1}{3}\left(\frac{\sigma}{r_c}\right)^{3}\right] \tag{3}$$

This can be evaluated instantly analytically; it is close to ideal for a system of identical particles and still works quite well for general systems when using average parameters. Since the dispersion term is much stronger than repulsion, it is typically limited to a dispersion correction

$$U_{\mathrm{dc}} = -\frac{8N\pi\rho\langle C^{(6)}\rangle}{3r_c^3} \tag{4}$$

where we have introduced the average dispersion parameter $\langle C^{(6)}\rangle$ for all particles in the system. Long-range corrections have been shown to be a significant improvement for many properties, and it is particularly important for more accurate free energy calculations.[11]

Unfortunately, the assumption made in the dispersion correction is formally only valid if the system is homogeneous and isotropic beyond the cutoff, and it fails for anisotropic systems such as lipid bilayers or other types of interfaces.[12] This has received less attention than electrostatics, but the adverse effects on lipid bilayer properties have been pointed out in several studies.[5,11,13,14]

The practical issue has earlier been addressed by Lagüe and co-workers, who developed a pressure based long-range correction (LRC) for LJ-interactions.[15] LRC applies an additional pressure, ΔP, calculated from the instantaneous pressure-difference between the simulated system at a cutoff either specific to the simulation or much longer, thus increasing density and decreasing isothermal compressibility. The method has been shown to be mostly independent of the specific cutoff and is available in the CHARMM simulation package.[16] Another recent contribution is the extension of the isotropic periodic sum (IPS) method developed by Wu and Brooks,[17] in order to also handle long-range dispersion interactions.[14,18,19] In IPS, the long-range interactions are handled by an isotropic sum over imaginary images of all the particles inside a defined homogeneous region, which can be extended to multiples of the longest edge of the simulation box. IPS makes it possible to treat an inherently heterogeneous system as a homogeneous one, thereby enabling the calculation of the long-range contributions to the dispersion energy by summing over the isotropic periodic images. It also presents a possibility to remove periodicity effects from the calculated long-range interactions, if the homogeneous region can be defined inside the simulation box.

However, already the classical smooth PME paper by Essmann et al.[10] suggested that more general forms of long-range interactions in theory could be handled with PME. The authors noted that the lattice summation algorithm can be generalized to handle any interaction on the form $r^{-\alpha}$ with $\alpha \geq 1$ and showed how this could be applied to dispersion interactions. Despite this, PME applied to long-ranged Lennard-Jones (LJ-PME) interactions has largely not been implemented or used in any normal simulations since the method becomes more complicated (and this far it has been very slow) when there are different particle types involved. This is tied to the problem of deriving interaction parameters for mixed particle types, and the combination rules typically employed for Lennard-Jones interactions. Compared to a single-particle-type system, these combination rules usually increase the amount of work much more than the simple charge product in electrostatics, and in many of these cases, the method becomes prohibitively computationally expensive.

In this paper, we present a new implementation of PME for Lennard-Jones interactions and examine the properties as well as assess the aforementioned severity of the artifacts from typical dispersion-corrected cutoffs on bilayer systems. Results from three different simulations of liquid pentadecane indicate that the method is compatible with present force fields when the system is homogeneous, and differences in the observables typically used for parametrization (density and heat of vaporization) are within the statistical errors. Since pentadecane is a model compound to derive parameters for lipids, this confirms previously developed lipid parameters should be fully transferable, but with LJ-PME significantly improving accuracy for anisotropic and inhomogeneous systems. Simulations of palmitoyl-oleoyl-phosphocholine (POPC) and dipalmitoyl-phosphocholine (DPPC) lipid bilayers result in differences in area per lipid of up to 5.5% compared to simulations using cutoffs for Lennard-Jones interactions. These effects are significantly larger than the differences the community historically has tried to address with improved parametrization, which, in our opinion, means we should reconsider the practice of using cutoffs for Lennard-Jones interactions in systems that are highly anisotropic and inhomogeneous; there is a strong case for using lattice summation for nonpolar interactions, too. We also propose a solution to the performance problems related to combination rules for realistic biomolecular systems with multiple different particle types, and show that this yields an increase in performance by almost 300% over the reference case.

2. THEORY

2.1. Combination Rules. In order to describe the LJ interaction between two atoms, i and j, the interaction parameters $C_{ij}^{(12)}$ and $C_{ij}^{(6)}$, or σ_{ij} and ε_{ij} are required. Force fields describing the interaction with $C_{ij}^{(12)}$ and $C_{ij}^{(6)}$ typically do this by using a geometric mean of the respective values for atom i and j,

$$C_{ij}^{(6)} = (C_i^{(6)}C_j^{(6)})^{1/2} \qquad C_{ij}^{(12)} = (C_i^{(12)}C_j^{(12)})^{1/2} \tag{5}$$

Some force fields employing σ_{ij} and ε_{ij} also use geometric averaging, although the most common approach is the use of

so-called Lorentz−Berthelot (LB) combination rules that derive the distance parameter σ_{ij} from an arithmetic mean and ε_{ij} geometrically

$$\sigma_{ij} = \frac{1}{2}(\sigma_i + \sigma_j) \qquad \varepsilon_{ij} = (\varepsilon_i \varepsilon_j)^{1/2} \tag{6}$$

This use of an arithmetic mean for the distance parameter is usually a better approximation of the excluded distance between two atoms of different size.

When applying the PME algorithm, the type of combination rules used for the specific interaction has a major effect on the performance of the simulation. As shown in the work of Essman et al.,[10] the reciprocal part of $r^{-\alpha}$ interactions will be dependent on the evaluation of

$$\sum_i \sum_j C(i, j)\exp[-2\pi i \mathbf{m}(\mathbf{r}_i - \mathbf{r}_j)] \tag{7}$$

where $C(i, j)$ represents the parameter specific to the type of interaction and $\mathbf{m}$ is the reciprocal lattice vector. For electrostatic interactions, this interaction parameter is simply the product of the two point charges: $C(i, j) = q_i q_j$, which thereby allows $C(i, j)$ to be factorized, and the reciprocal energy sum can be expressed in terms of structure factors

$$S(\mathbf{m}) = \sum_j^N q_j \exp[2\pi i \mathbf{m}\cdot\mathbf{r}_j] \tag{8}$$

When using LJ-PME together with geometric combination rules, the methodology translates directly to $C(i, j) = \sigma_i^{1/2}\sigma_j^{1/2}$, and this makes it straightforward to use LJ-PME when this type of force field combination rule is applied. However, when the applied force field utilizes the LB combination rules things get more complicated since $C(i, j)$ now splits into seven terms according to

$$C(i, j) = (\sigma_i + \sigma_j)^6 = \sum_{n=0}^{6} P_n \sigma_i^n \sigma_j^{(6-n)} \tag{9}$$

where P_n represents the Pascal triangle coefficients. It is not possible to factorize this in any simple fashion, and therefore, the reciprocal dispersion energy and structure factors have to be expressed as seven terms

$$\begin{aligned} S(\mathbf{m})S(-\mathbf{m}) &= \sum_{i,j}\sum_{n=0}^{6} P_n \sigma_i^n \sigma_j^{(6-n)} \exp(2\pi i \mathbf{m}(\mathbf{r}_i - \mathbf{r}_j)) \\ &= \sum_{n=0}^{6} P_n [\sum_i \sigma_i^n \exp(2\pi i \mathbf{m}\cdot\mathbf{r}_i)] \\ &\quad [\sum_j \sigma_j^{(6-n)} \exp(-2\pi i \mathbf{m}\cdot\mathbf{r}_j)] \\ &= \sum_{n=0}^{6} P_n Z_n(\mathbf{m}) Z_{6-n}(-\mathbf{m}) \end{aligned} \tag{10}$$

with $Z_\alpha(\mathbf{m}) = \Sigma_j \sigma_j^\alpha \exp(2\pi i \mathbf{m}\cdot\mathbf{r}_j)$. This severely increases the computational load when evaluating the structure factors in the PME algorithm, since it requires seven separate FFTs, and hence, the performance is drastically decreased for this type of force field. In the past, this has been the largest problem with implementing LJ-PME, since the gain in accuracy has not been worth the huge loss of performance inherent to the method. In this context, it should also be noted that force fields not employing combination rules or using exceptions[20] for nonpolar interaction parameters cannot be handled exactly with LJ-PME.

3. METHODS

3.1. Pentadecane Simulations. As an example of a homogeneous and isotropic system relevant for lipid parametrization, a system with 128 united-atom pentadecane molecules in a box of size 40 × 40 × 40 Å was generated by removing hydrogens from an all-atom configuration. Relaxation of the system was carried out by steepest descent minimization, after which it was simulated for 10 ns using a time step of 2 fs while constraining all bond lengths with the LINCS[21] algorithm. The temperature was maintained at 298 K using the Berendsen weak coupling algorithm,[22] and the pressure was kept at 1 bar using the Parrinello−Rahman barostat.[23] Parameters from Berger,[24] Chiu,[25] and Ulmschneider[13] were used to describe the interactions between pentadecane molecules in three separate simulations. Each system was simulated once with the truncation of the long-range Lennard-Jones interactions specified for the force field used and once with all nonpolar interactions treated with LJ-PME. For the simulations with truncated interactions, cutoffs were set to 10 Å for the simulations with the Berger parameters. For the other simulations, twin-range cutoffs of either 10/14 Å (Ulmschneider) or 10/16 Å (Chiu) with a long-range update frequency of 10 steps where used, according to the proposed setups for these parameters. To calculate the heat of vaporization, simulations of a single pentadecance molecule in vacuum using a stochastic dynamics integrator with a time constant of 0.5 ps were also performed.

3.2. Lipid Bilayers. For the lipid bilayer simulations, equilibrated patches of 100 DPPC molecules and 3205 SPC/E[26] water molecules were generously supplied by Chiu,[25] and equilibrated patches of 128 POPC molecules and 5262 SPC[27] water molecules were obtained from the work of Hub et al.[28] The systems were simulated for 200 ns at 323K (DPPC) and 298K (POPC) respectively, using a time step of 2 fs. Bond lengths were constrained with the LINCS algorithm. Frames after 100 ns of simulation time were also used as starting configurations for constant area simulations with a total simulation time of another 100 ns for each system. Temperature was coupled with the Nosé−Hoover thermostat, and pressure was coupled semi-isotropically at 1 bar with the Parinello−Rahman barostat. DPPC parameters were taken from Chiu,[25] and the POPC parameters were modified from the parameters of Berger[24] by using parameters for the double bond and atom types from the OPLS united atom force field.[29] Electrostatic interactions were evaluated every step using PME,[10] and LJ-interactions were evaluated every step with LJ-PME or using a cutoff of either 10 Å (POPC) or a twin-range 10/16 Å cutoff updated every 10th step (DPPC). The combined LJ parameters were constructed with LB combination rules in the POPC simulation, while the DPPC system used geometric combination rules. A DPPC monolayer was constructed by translating a bilayer in the z-direction until the periodic boundary was positioned in the middle of the bilayer. Then, the box was extended in the z-direction by 15 Å in order to separate the two leaflets and create two lipid/vapor interfaces. This system was equilibrated for 10 ns at a constant volume, and otherwise, it used the same settings as the DPPC bilayer. Finally, two 50 ns simulations were performed, one with truncated LJ-interactions and one with LJ-PME.

3.3. Umbrella Simulations. The free energy profile for a propane molecule in a POPC bilayer was calculated by using umbrella sampling. The position along the membrane normal (z-axis) was chosen as a reaction coordinate, with the $z = 0$ position at the center of the lipid bilayer. Starting structures were created by pulling a propane molecule across the simulation box of a POPC membrane during a 30 ns simulation. For simulations performed with LJ-PME, the starting structure of the POPC bilayer was taken from the last frame in the corresponding bilayer simulation, and for the simulations with truncated LJ-interactions the structure was taken from the POPC simulation using a 10 Å cutoff. Umbrella windows were positioned with a distance of 0.2 Å between adjacent windows, using 315 windows for the cutoff simulations and 332 for the simulations using LJ-PME. The umbrella potential was harmonic with a force constant of 4000 kJ mol^{-1} nm^{-2} applied to the center-of-mass of the propane molecule, and each window was first equilibrated for 2 ps and then simulated for 3 ns using the same simulation parameters as in the simulations of the pure bilayers, with the exception that temperature was controlled using a stochastic dynamics integrator with a time constant of 0.1 ps.

Potential of mean force (PMF) curves were computed using a periodic version of the weighted histogram analysis method (WHAM),[30] which is implemented in the g_wham[31] module of Gromacs. The first nanosecond of simulation time was considered relaxation and removed from each umbrella window, and the two PMFs were created from the umbrella histograms. The integrated autocorrelation times of the separate umbrella windows were incorporated in the WHAM iterations, and smoothened along the reaction coordinate using a Gaussian with $\sigma = 0.2$ nm. In order to reduce the statistical error, PMFs were symmetrized around $z = 0$.

All simulations were carried out with a modified development version of the Gromacs simulation package (4.5.2), which is freely available at ftp://ftp.gromacs.org/pub/ljpme/.

4. RESULTS

4.1. Parameters Are Transferable to LJ-PME. With the introduction of PME for electrostatics, a central question was whether the then-current force fields needed to have charges reparameterized in order to be compatible with PME. Overall, there were few or no difficulties in using PME electrostatics together with the existing force fields. Still, in some specific cases, especially regarding water,[6,32] PME had a non-negligible effect on the simulated properties since its charges had been specifically tuned to reproduce experimentally derived properties at a specific short (usually 9 Å) cutoff. In analogy, we first wanted to validate that the liquid pentadecane properties typically used to parametrize bilayers are not affected by the introduction LJ-PME, which is necessary to be able to reuse current force fields. For this purpose, a test simulation of pure liquid pentadecane was chosen as a model of an isotropic and homogeneous system, for which the classical dispersion correction used during parametrization should be a reasonably accurate approximation. To make existing parameters transferable to LJ-PME, the differences between properties from truncated interactions and LJ-PME simulations should be small. The properties that are normally used for parametrization of LJ-parameters are the heat of vaporization and the density of hydrocarbons,[24] making these the most important observables to validate between methods.

The g_energy module of the Gromacs simulation package was used to calculate the density from the simulations. The heat of vaporization, ΔH_{vap}, was calculated as

$$\Delta H_{vap} = E(\text{gas}) - E(\text{liquid}) + NkT \tag{11}$$

where E(liquid) is the energy per molecule in a simulation of liquid pentadecane, k the Boltzmann constant, N the number of pentadecane molecules in the simulation, and T the temperature. E(gas) was calculated from a simulation of a single pentadecane in vacuum.

The calculated heat of vaporization and density from the pentadecane simulations, averaged over the last 5 ns, are listed in Table 1. For these simulations, three different force field parameters were used: the Berger parameters[24] commonly used in simulations of lipid bilayers, a recent update to the GROMOS 43A1 force field by Chiu et al.,[25] and a new parameter set compatible with the OPLS-AA protein force field[33] developed by Ulmschneider,[13] all with different cutoff schemes, as described in the methods section. It should be noted that the Berger parameters suffered from an outdated or incorrect value of the heat-of-vaporization in the 54th edition of the CRC handbook when they were derived, and the GROMOS force field does not strictly use combination rules, although this does not apply to the lipid parameters used here. Since our interest here is to validate the LJ-PME methodology rather than force fields, the table also lists the corresponding reference values each force field was parametrized against. In the work of Berger et al., experimental and simulation volume per pentadecane was reported rather than density, but for

Table 1. Calculated Heat of Vaporization and Density of Liquid Pentadecane from Simulations Carried out Using Three Different Force Field Parameters[a]

Berger		
method	heat of vaporization [kJ/mol]	density [kg/m^3]
cutoff	63.4 ± 0.2	760.7 ± 0.3
LJ-PME	63.4 ± 0.2	761.0 ± 0.2
reference	61.2	752
Chiu		
method	heat of vaporization [kJ/mol]	density [kg/m^3]
cutoff	79.1 ± 0.2	776.4 ± 0.2
LJ-PME	79.1 ± 0.2	776.8 ± 0.2
reference	76.8	764.8
Ulmschneider		
method	heat of vaporization [kJ/mol]	density [kg/m^3]
cutoff	76.0 ± 0.2	787.2 ± 0.2
LJ-PME	76.0 ± 0.2	787.6 ± 0.2
reference	72.8	765.0

[a]The reference lines correspond to the values originally used to parametrize each force field for smaller systems, rather than the currently most recent experimental value; in particular, for Berger, there is a significant difference since those authors used an older version of the CRC handbook. For the Berger and Ulmschneider force fields, full Lorentz−Berthelot LJ-PME was used, while Chiu is specified to use geometric rules. The close agreement confirms that the parameters derived using cutoffs from isotropic and homogenous systems (where the dispersion correction approximation holds) should be equally valid and accurate when used in combination with lattice summation of the dispersion correction—normal force fields derived from simple liquids will not have to be reparametrized to be used with LJ-PME.

convenience, all values have been converted to density here. For all three setups, there are no statistically significant differences in the heat of vaporization or density related to the usage of LJ-PME vs cutoffs—the largest relative deviations are in the order of 0.03%, which is far below the standard error. We also evaluated the isothermal compressibility from the volume fluctuations (directly available in the Gromacs g_energy tool); for the Berger force field, this was 1.1×10^{-4} bar^{-1} both with LJ-PME and cutoffs, for the Chiu parameters, the values are 7.4×10^{-5} bar^{-1} (LJ-PME) and 7.3×10^{-5} bar^{-1} (cutoff), and finally, for Ulmschneider, they are 7.9×10^{-5} bar^{-1} and 8.3×10^{-5} bar^{-1}, respectively. These variations are likely within the statistical errors, in particular, when compared to the difference to the experimental value[34] (9.1×10^{-5} bar^{-1}). The variation between the force fields is likely due to their different torsion potentials.

The good agreement between values calculated with either truncated LJ-interactions and dispersion corrections or lattice summation indicates that treating homogeneous systems with PME instead of cutoffs does not alter the properties of the simulated systems, despite the fact that the force fields are frequently parametrized to be used together with specific cutoffs for the long-range LJ-interactions, and the summation of all periodic copies inherent to PME could lead to artificial ordering.

As pentadecane is one of the larger hydrocarbons to test this implementation on, the results obtained suggest that LJ-PME should also be as accurate for systems containing smaller molecules. This also seems to be the case from similar tests on homogeneous and isotropic systems performed for IPS[14] (including smaller molecules), although the evaluation of the long-range virial tensor to evaluate pressure is different. Nevertheless, these results constitute an important validation of the implementation: it shows that LJ-PME is sufficiently compatible with the lipid force fields tested, and it is at least likely to extend to other force fields as well.

4.2. LJ-PME Has a Clear Effect for Anisotropic Systems. The strength of LJ-PME lies in its ability to correctly describe the effects on systems were the dispersion correction approximations fail, in particular, systems that are highly anisotropic and inhomogeneous. For this, two different lipid bilayers, with DPPC and POPC lipids, were simulated and used to compare mechanical bilayer properties. Although we primarily analyzed area per lipid in constant-pressure simulations, a second set of simulations with constant volume were used to calculate surface tensions to facilitate comparisons with other works in the literature. For the simulations using pressure coupling, the area per lipid was calculated by dividing the area of the simulation box with the number of lipids in each leaflet. Similarly, in the constant area simulations, the surface tension γ was calculated as

$$\gamma = \frac{1}{2}(P_{zz} - 0.5(P_{xx} + P_{yy}))/L_z$$

where P_{xx}, P_{yy}, and P_{zz} are the components of the pressure tensor in the directions along the bilayer surface (x and y) and parallel the bilayer normal (z), while L_z is the height of the simulation box. Table 2 lists the properties calculated from both constant-pressure and constant-area bilayer simulations compared to experiments,[35−37] and Figure 1 illustrates the variation in area per lipid during the constant-pressure simulation.

For the DPPC system, the simulation with pressure coupling using truncated LJ-interactions produced an area per lipid of 62.9 Å^2, which agrees well with the value of 63.6 Å^2 reported by Chiu et al.[25] under similar conditions. Despite the fact that this setup uses a remarkably long cutoff of 16 Å for LJ-interactions, the area per lipid is still significantly lower (61.4 Å^2) in the simulation where nonbonded interactions are evaluated with LJ-PME. Apart from a few minor fluctuations, this difference

Table 2. Properties of Constant-Pressure and Constant-Area DPPC/POPC Bilayer Simulations with and without LJ-PME[a]

bilayers	constant-pressure	constant-area
DPPC	area/lipid [Å^2]	surface tension [mN/m]
cutoff	62.9 ± 0.3	−4.0 ± 0.9
LJ-PME	61.4 ± 0.2	−2.5 ± 2.7
experiment[37]	63.0	
POPC	area/lipid [Å^2]	surface tension [mN/m]
cutoff (10 Å)	71.0 ± 0.3	−10.2 ± 2.3
cutoff (16 Å)	68.8 ± 0.2	−1.2 ± 1.6
LJ-PME	67.1*	2.0 ± 1.7
experiment[36]	68.3	
monolayers		
DPPC		surface tension [mN/m]
cutoff		40.9 ± 1.2
LJ-PME		50.0 ± 1.2
experiment[35]		40.9

[a]Cutoff simulations used truncation at 10 Å (POPC) and 10/16 Å (DPPC) together with dispersion corrections. A longer cutoff of 16 Å was also tried for the POPC system, in order to check the extent to which this reduces the difference compared to LJ-PME simulations. The constant-pressure simulations were analyzed in terms of area per lipid (column 2) while the constant-area simulations were used to calculated a surface tension (column 3). For the latter case, the area per lipid was 60.9 Å^2 for DPPC and 67.5 Å^2 for POPC). There are significant effects on the bilayer properties that depend on the treatment of long-range dispersion interactions. For POPC, the LJ-PME simulation exhibited an area per lipid that was still decreasing after 200 ns, and although it is clearly different from the cutoff, this makes it impossible to estimate a reliable standard error (*).

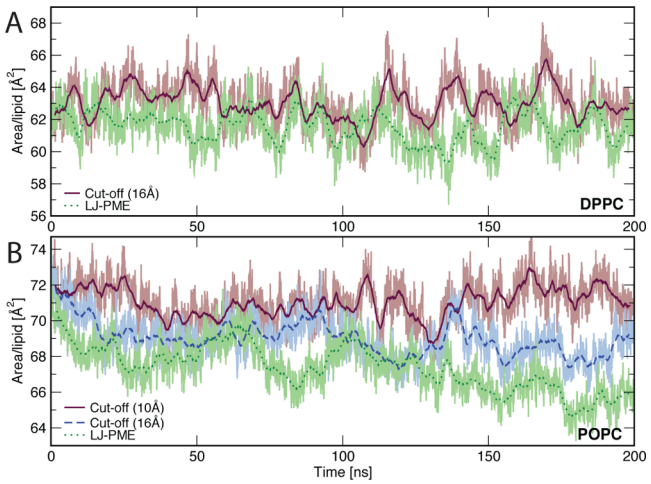

Figure 1. (A) Area per lipid calculated from two simulations of DPPC, using either cutoffs (solid) or LJ-PME (dotted) for nonpolar interactions. The simulation using cutoffs results in higher area/lipid, likely due to fewer attractive interactions. (B) For POPC lipids, the shorter cutoff at 10 Å (solid) results in a larger difference compared to the simulation using LJ-PME. Increasing the cutoff to 16 Å (dashed) reduces this difference to the same level as in the DPPC simulations.

dx.doi.org/10.1021/ct400140n | J. Chem. Theory Comput. 2013, 9, 3527−3537

between the cutoff and lattice summation setups is present throughout the 200 ns test simulation (Figure 1). Even for very long cutoffs, there appears to be a systematic difference between dispersion correction and proper inclusion of the weak but ubiquitous long-range nonpolar interactions. This indicates that treating nonbonded interactions with LJ-PME does indeed have an impact on the properties of inhomogeneous and anisotropic systems, and from the simulations of liquid pentadecane, we can also rule out the possibility that this discrepancy stems from an incompatibility of LJ-PME with the applied force field.

The constant-pressure simulations of POPC bilayers display largely the same effects as those seen for DPPC. For this force field, the default cutoff is shorter at 10 Å. The area per lipid calculated from the dispersion correction simulation is 71.0 Å^2, and this drops to 67.1 Å^2 with Lennard-Jones lattice summation enabled (Table 2, Figure 1). The relative change is much larger than for the DPPC system above, 4.8% compared to 2.4%. In fact, for at least one of the LJ-PME simulations, the area still appears to be decreasing after 200 ns (for this reason we do not estimate specific standard errors for this system). This larger effect can almost certainly be attributed to the shorter cutoff of 10 Å used for the POPC simulation compared to the twin range 10/16 Å cutoff used in the DPPC simulation. However, it should be noted that a 10 Å cutoff is a common standard for simulations of membrane proteins and other applications today, which means many of them could have quite significant inherent errors.

Since PME evaluates the full, infinite sum over all periodic images in the system, it is reasonable to believe that a twin-range 10/16 Å cutoff should decrease the difference compared to the LJ-PME simulation. To test this, a second identical POPC system was simulated with longer cutoffs under constant pressure, and as shown in Figure 1, this does indeed result in a lower area. The simulation with an increased cutoff showed a calculated area per lipid of 68.8 Å^2, which is a relative difference of 2.4%, which is of the same order as in the simulations performed with DPPC. Still, while the error is somewhat reduced with a longer cutoff, the complex geometry of the anisotropic system with different regions of hydrocarbon, headgroups, and water would likely require excessively long cutoffs to get close to the convergence we achieve by introducing LJ-PME.

4.3. LJ-PME Alters Bilayer Properties. The drop in area per lipid after introducing LJ-PME in the simulated bilayers appears to indicate increased attractive forces in the bilayer plane acting on each molecule from the long-range interactions that are neglected when using cutoffs. Due to the high correlation between area per lipid and order in bilayers, this will also have a direct effect on other properties of the system. Figure 2 illustrates experimental[38,39] and calculated deuterium order parameters, S_{cd}, for the lipid tails evaluated as

$$S_{cd} = \frac{2}{3}S_{xx} + \frac{1}{3}S_{yy}$$

with S_{xx} and S_{yy} defined according to

$$S_{ij} = \frac{1}{2}\langle 3\cos\theta_i \cos\theta_j - \delta_{ij}\rangle$$

where θ_i represents the angle between the ith molecular axis and the bilayer normal.[40]

The lattice summation of nonpolar interactions increases the order in the lipid tail region both for the DPPC and POPC simulations, which is coupled to straighter chains and the reduced area per lipid. Similar effects of increased order with longer standard cutoffs in bilayer simulations despite the usage of dispersion correction have previously been reported, for example, by Ulmschneider et al.[13]

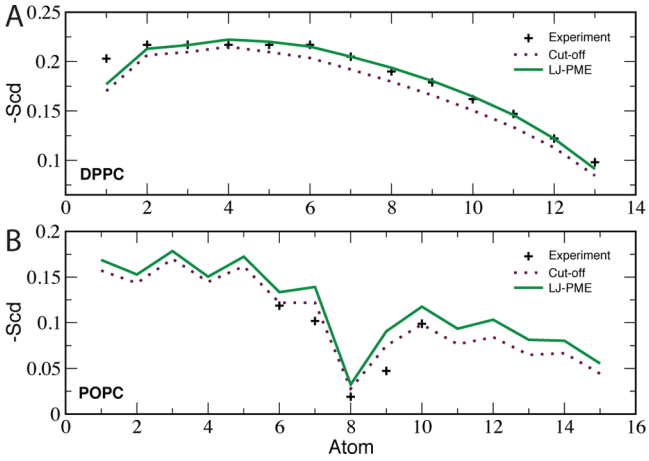

Figure 2. Deuterium order parameters calculated from simulations of DPPC (A) and the sn2 chain of POPC (B). The classical dispersion correction does not correctly account for the anisotropy of the long-range nonpolar interactions in bilayers, which leads to a non-negligible effect on the order in the bilayer due to the high correlation with area per lipid. The effect is somewhat stronger for the more ordered DPPC lipids, where it also results in a very close fit to the experimental values, although larger systems would be needed for truly accurate assessment of the agreement with experiments. Experimental values for DPPC and POPC are taken from refs 38 and 39.

The second column in Table 2 reports the surface tension calculated from the additional set of constant-area simulations. For DPPC simulated with truncated LJ-interactions, the calculated surface tension is −4.0 mN/m while the value obtained from the LJ-PME simulation is −2.5 mN/m. For POPC, this difference is much larger, with a surface tension of −10.2 mN/m in the cutoff simulation compared to 2.0 mN/m for the LJ-PME simulation. When the cutoff is increased to 16 Å, this difference decreases as the surface tension then changes to −1.2 mN/m for the first setup. Venable et al.[14] did not observe any significant differences in surface tension between simulations using IPS or LJ-interactions truncated at 12 Å, although Klauda still find a difference for CHARMM36 at this cutoff.[12] For LJ-PME and the present force fields, such a 12 Å cutoff would not be sufficient to remove the discrepancy; even at the 16 Å cutoff we see a statistically significant difference in the calculated area per lipid compared to those obtained from the simulation with LJ-PME.

In addition to this, we also performed simulations on DPPC monolayers (Table 2) at an area of 63.8 Å^2, using both LJ-PME and a twin-range 10/16 Å cutoff. Previous work by both Klauda et al.[12] and Venable et al.[14] observed an inconsistency in the obtained surface tensions from mono- and bilayer simulations with and without long-range dispersion forces included. We see the same effect in our simulations, with the monolayer displaying an increased surface tension of almost 25% when using LJ-PME. Following the same conclusions drawn by Venable et al. regarding the C27r force field,[41] this suggests that the very good agreement with experimental values obtained with the GROMOS 43A1-S3 force field could be due to cancellation of errors.

Furthermore, as a demonstration of the effect LJ-PME could have on a common simulation procedure, we performed two sets of simulations in which umbrella sampling was used to measure the potential of mean force (PMF) for the permeation of propane across a POPC bilayer (Figure 3). As would be

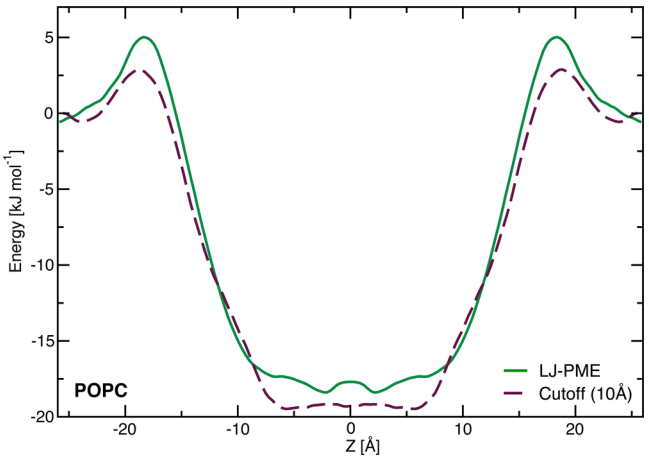

Figure 3. Symmeterized PMFs of the permeation of propane across a POPC bilayer, calculated using either LJ-PME (solid green) or a cutoff of 10 Å (dashed red). In the LJ-PME simulation the PMF displays a higher permeation barrier both at the lipid headgroup and tail regions, due to the decreased area per lipid (Figure 1) and the increased ordering (Figure 2) of the lipid tails present in the simulation. The PMFs are smoothened using a running average over 10 points.

expected from the discrepancy in the area per lipid in the two structures (Figure 1), we see a higher permeation barrier in the LJ-PME simulations with a peak in the headgroup region of 5.0 ± 0.5 kJ mol^{-1}. For the cutoff simulation, this peak is slightly lower at 2.9 ± 0.6 kJ mol^{-1}, but the difference is still statistically significant even for a small molecule such as propane. There is also a small free energy difference in the lipid tail region, where the increased ordering of the lipid chains (Figure 2) makes the environment marginally less favorable for propane in the LJ-PME bilayer. However, this difference is not as significant as the one present in the headgroup region, since the standard error of the cutoff simulation is approximately 2.8 kJ mol^{-1} in the region between $z \approx \pm 10$ Å (0.9 kJ mol^{-1} for the LJ-PME simulation). Albeit a rather simple test case, we believe these simulations show that the addition of long-range dispersion interactions can have an important effect on properties related to the membrane structure.

4.4. Effects of Combination Rule Approximations. The greatest concern when using LJ-PME is how to handle the expensive calculations coupled to the simulations in which the common Lorentz−Berthelot combination rules are used. Some performance benchmarks are shown in Table 3. A comparison between the two different simulations illustrates the impact different combination rules have on the performance of LJ-PME: In the DPPC simulation setup, which uses geometric combination rules, LJ-PME is only about 25% slower than the corresponding cutoff simulation at 61.2 ns/day compared to 80.6 ns/day. In this context, it should be noted that we are comparing against the heavily tuned standard implementation of PME electrostatics and nonbonded cutoffs in GROMACS, not a slower reference setup. In the POPC simulations, which uses LB combination rules, LJ-PME predictably performs much worse by only achieving 18.9 ns/day, which leaves it at a

Table 3. Performance from Running Simulations of POPE and DPPC in Gromacs-4.5.2[a]

DPPC		
method	no. processors	ns/day
cutoff (16 Å)	168	80.6
LJ-PME	168	61.2
POPC		
method	no. processors	ns/day
cutoff (10 Å)	120	80.1
cutoff (16 Å)	120	67.8
LJ-PME	120	18.9

[a]For the geometric combination rules employed in the Chiu force field (DPPC), the performance difference is quite reasonable considering the improved accuracy, but when the force field relies on Lorentz−Berthelot (POPC) combination rules, as is most common today, there is a severe performance loss which would make the approach largely unusable in practical simulations if the lattice part has to use exact combination rules. Simulations were carried out on AMD Opteron 6238 CPUs.

performance loss of ∼72% even compared to the simulation with a longer 16 Å cutoff for nonpolar interactions.

This leaves much to ask for when it comes to the performance of LJ-PME, especially for force fields using LB combination rules where we would classify the default performance as borderline uninteresting. On the other hand, as we have shown in this work the effects of this on the properties of inhomogeneous systems is actually larger than differences that are frequently the target of reparameterizations today. This indicates that a correct treatment of all the long-range interactions is necessary as the next step in order to increase the accuracy of simulations in general, and bilayer simulations in particular. If one could overcome the inherently low performance of LJ-PME for systems with LB combination rules it would be a natural method of choice since PME is already routinely used for electrostatics.

As a possible solution to this performance problem, we propose an approximation where the interactions calculated in reciprocal space are treated with geometric combination rules, even when the applied force field actually specifies Lorentz−Berthelot rules. While this might seem like a major change at first, it is actually very limited. First, since the real and reciprocal parts of the potential can be defined separately and they both fulfill the conditions of conservative potentials with well-defined Hamiltonians, their sum will also fulfill these criteria despite using different combination rules for the two parts. Second, since the lattice summation gradually switches off direct space interactions and gradually switches on reciprocal space interactions as the interaction distance increases, there will not be sudden changes in the potential at any point. Third, the difference between various combination rules primarily enters at very short distances, while it is much smaller for the interactions treated in reciprocal space. Thus, while the approximation admittedly will introduce small errors in the energy of the system, we show below that this will be a negligible change in the total energy, since the contribution from the reciprocal part is very small compared to the real space contribution.

Figure 4A illustrates all parts (real, reciprocal, and total) of a calculated dispersion potential for the interaction between phosphorus and oxygen, with parameters taken from the Berger force field, a real space cutoff of 10 Å and LB combination rules

dx.doi.org/10.1021/ct400140n | J. Chem. Theory Comput. 2013, 9, 3527−3537

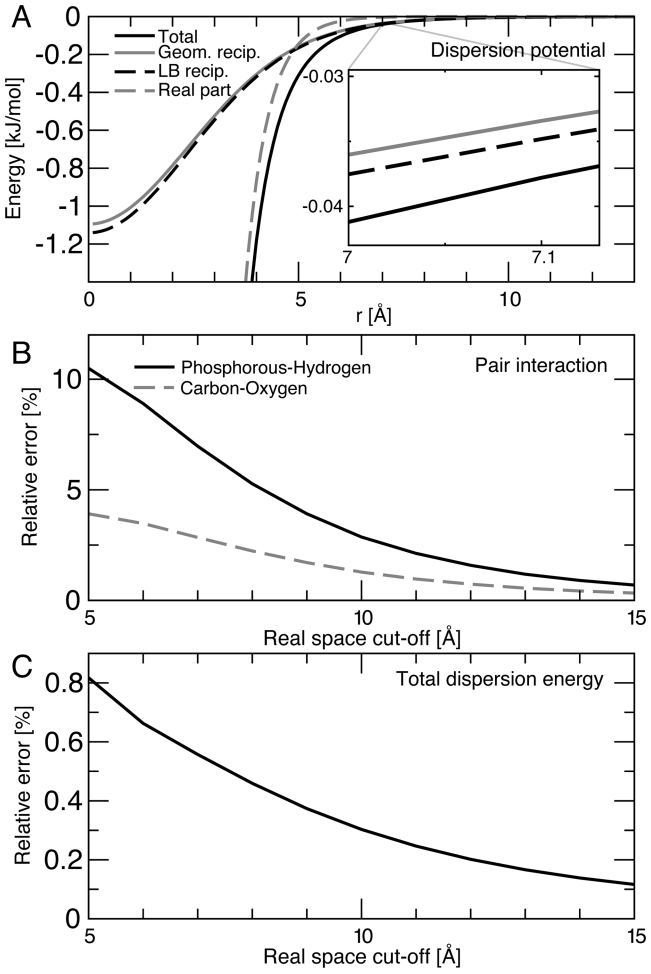

Figure 4. (A) Dispersion potential between phosphorus and oxygen. Direct-space (dashed gray) and reciprocal (dashed black) parts of the total (solid black) dispersion for Lorentz−Berthelot (LB) rules. Approximating the reciprocal contribution with geometric rules (solid gray) introduces a small error. (B) Integrated total deviation of dispersion interactions with geometric reciprocal space combination rules compared to full LB rules, for phosphorus−hydrogen (solid black) and carbon−oxygen (dashed gray), as a function of direct-space cutoff. (C) Relative difference for the total dispersion potential for a POPC bilayer using geometric reciprocal space rules compared to LB, as a function of direct-space cutoff. The relative error is kept below 0.5% even at a cutoff of 8 Å.

applied. In addition to this, the reciprocal potential calculated with geometric combination rules is also shown. The total error introduced when approximating the reciprocal contribution with geometric combination rules can be calculated as the difference between the two reciprocal potentials

$$E_{\mathrm{err}} = \int_{\sigma_{ij}}^{\infty} (E_{\mathrm{recip}}{}^{\mathrm{LB}} - E_{\mathrm{recip}}{}^{\mathrm{geom}})\mathrm{d}r \qquad (12)$$

where $E_{\mathrm{recip}}{}^{\mathrm{LB}}$ and $E_{\mathrm{recip}}{}^{\mathrm{geom}}$ represent the reciprocal energy calculated with LB or geometric combination rules, and the lower integration limit is chosen as σ_{ij} since the dispersion term is negligible compared to the repulsive part of the LJ-potential at short distances.

Figure 4B shows this error related to the total dispersion energy plotted against the applied real space cutoff for two different pair interactions with relatively large differences in their respective values of σ, thereby yielding significant differences in σ_{ij} depending on the applied combination rule. The resulting relative errors are quite large for short real space cutoffs, up to 10%, but one should keep in mind that this only concerns the reciprocal space nonpolar interactions—once the direct space dispersion and repulsion are taken into account, it will be much smaller. At the commonly used cutoff of 10 Å, the relative error for the (in this regard) extreme interaction between phosphorus and hydrogen (a relative difference in C_{ij}^{6}-values of approximately 11%) is 2.8%, which in absolute terms corresponds to an energy difference of 0.002 kJ/mol. For the interaction between carbon and oxygen, the relative difference in $C_{ij}^{(6)}$ values is smaller (4.1%), thereby reducing the relative error to 1.2% at a cutoff of 10 Å, which as in the previous case also corresponds to 0.002 kJ/mol due to the stronger interaction between carbon and oxygen. In our opinion, these differences are far below the accuracy in the parametrization of the force fields, and it is important to remember that we are comparing it to the ideal case of complete Lorentz−Berthelot combination rule lattice summation—the standard approach of brute truncation and analytical dispersion correction used in most current simulations is a far worse approximation.

While the extreme cases are useful to analyze worst-case effects, it is also useful to assess the effect on a realistic system. Figure 4C displays the relative error in the total dispersion energy for a system containing the POPC bilayer (see the Methods). Since the majority of the atoms in a bilayer system have relatively similar σ-values, the error introduced by approximating the reciprocal energy is very small. For this specific case, we attain a relative error of less than 0.5% already at a real space cutoff of 8 Å. When including the direct space dispersion and repulsion, the total error is below 0.1% compared to full Lorentz−Berthelot LJ-PME.

This modified version of the PME methodology was tested on the POPC bilayer, and results can be seen in Table 4 and

Table 4. Calculated Properties and Performance for LJ-PME Simulations Using the Full Exact Lorentz−Berthelot Combination Rules vs the Approximation Using Geometric Combination Rules in Reciprocal Space[a]

bilayer properties		
method	area/lipid [Å^2]	surface tension [mN/m]
LB combination rules	67.1 ± 0.2	2.0 ± 1.7
geometric combination rules	66.7 ± 0.4	2.4 ± 2.9
performance		
method	no. processors	ns/day
full LB comb. rules	120	18.9
geometric recip. comb. rules	120	52.5

[a]The difference between the two results is not statistically significant; assessing the difference as a function of time, the average is 0.43 Å^2 with a standard error of 0.76 Å^2. In contrast, both LJ-PME runs deviate markedly from the truncation and dispersion correction results in Table 2, while the geometric approximation achieves almost the same performance as truncation.

Figure 5. The difference in calculated area per lipid is 0.4 Å, and the difference for the surface tension is 0.4 mN/m. These differences relative to full LB LJ-PME are not statistically significant, but even if they had been, we would like to stress that the important analysis is to compare with Table 2—compared to cutoffs, the combination rule approximation is strikingly close to the full Lorentz−Berthelot LJ-PME reference case. However, in contrast to the reference case, this

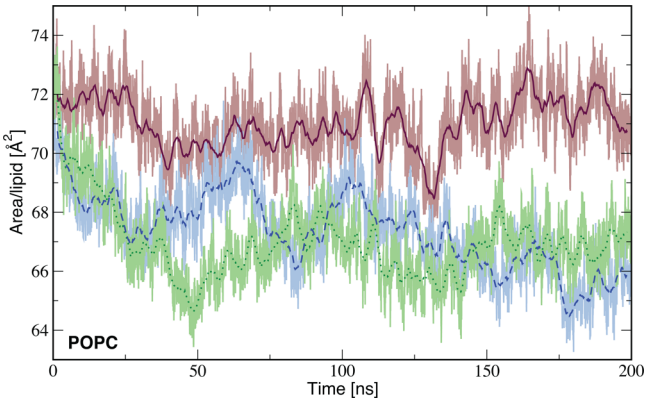

Figure 5. Calculated area per lipid from simulations of POPC, using either a 10 Å cutoff (solid), full exact LB combination rules (dotted), or reciprocal space geometric combination rules (dashed). Both LJ-PME simulations deviate significantly from the cutoff simulation, while the difference between them is not statistically significant (Table 4).

approximation achieves a performance improvement of ∼280%. Using geometrical combination rules in reciprocal space, we reach 52.5 ns/day compared to only 18.9 ns/day for the reference LB LJ-PME setup, which is only 20% slower than simulations using twin-range cutoffs. Furthermore, Table 5

Table 5. Scaling Efficiency of the Current Implementation for the Small POPC System for the Three Different Simulation Setups Used in This Work[a]

	no. processors			
	16	32	64	128
geometric combination rules	1	1.8	2.9	3.9
LB combination rules	1	1.7	2.6	3.3
cutoff (10 Å)	1	2.0	2.9	5.7

[a]For the current implementation, LJ-PME experiences a communication-related drop in scalability when there is less than ∼500 particles per processor. Future development should reduce this and bring it closer to the scalability of current cutoff implementations. The scaling efficiency was measured using Intel E5-2660 CPUs.

shows a comparison of the relative scalability of the three different simulation setups. The simulation with geometric combination rules scales almost as well as the cutoff simulation up to 64 cores, while the setup using LB combination rules performs slightly worse already at 32 cores. The large difference seen between LJ-PME and cutoff after 64 cores is coupled to the current implementation in Gromacs, which performs separate fast Fourier transforms (FFT) of the reciprocal grids for the electrostatic- and LJ-interactions. This makes communication a very prohibiting factor when running on a large amount of cores, and future development includes combining these calculations into a single strided FFT grid.

In addition to the numbers presented, Figure 5 illustrates calculated areas per lipid. The two LJ-PME simulations quickly drop in area per lipid to stabilize around 67 Å^2, and apart from fluctuations, no large differences are visible. Together with Table 4, these results indicate that by approximating the reciprocal space with geometric combination rules we substantially increase the performance of LJ-PME, and the errors coupled to this approximation are statistically insignificant compared to the standard deviations of the simulations using full LB combination rules in both real and reciprocal space.

4.5. Accuracy. RMSD-values of the total force, ΔF, were calculated for different spacings of the reciprocal grid and compared to a reference system using a grid spacing of 0.02 nm. Analogous to electrostatics PME, the real space scaling factor $g(\beta|r|)$ was set to be less than a specific tolerance $\varepsilon_{LJ} = 0.001$ at the real space cutoff, with the real space factor in LJ-PME being $g(x) = \exp(-x^2)(1 + x^2 + x^4/2)$. Table 6 shows the most

Table 6. Accuracy Calculations for the Two Lipid Systems Simulated in This Work[a]

DPPC				
grid spacing [nm]	0.05	0.1	0.15	0.2
ΔF [kJ mol^{-1} nm^{-1}]	0.020	0.18	1.05	3.40
β [nm^{-1}]	3.39	3.39	3.39	3.39
POPC				
grid spacing [nm]	0.05	0.1	0.15	0.2
ΔF [kJ mol^{-1} nm^{-1}]	0.015	0.18	1.21	3.43
β [nm^{-1}]	3.51	3.39	3.51	3.51

[a]RMSD values of the total force, ΔF, were calculated using a reference system with a reciprocal grid spacing of 0.02 nm, and fourth-order spline interpolation. The β value corresponds to the PME direct vs reciprocal space splitting parameter.

accurate RMSD-values, together with the value of the corresponding splitting parameter, β, calculated for the lipid bilayer systems used in this work. For the parameters investigated here, we obtain a fairly good accuracy for grid spacings up to 0.15 nm, and a value of β corresponding to a tolerance of approximately 8×10^{-4}. From this, we can also assess the accuracy of the simulations carried out in this work, which were performed using a grid spacing of 0.12 nm and a tolerance of 0.001.

5. CONCLUSIONS

Truncation of long-range LJ-interactions has a non-negligible effect on the properties of inhomogeneous and anisotropic systems. Comparison of the calculated properties from simulations using truncated LJ-interactions with those from simulations using LJ-PME shows differences in area per lipid of up to 5.5%. This indicates that the neglected interactions in simulations with truncated potentials do have a substantial effect on the bilayer properties and that a correct representation of these interactions are of great relevance for the development of future force fields. Although current force fields have been developed using cutoffs for LJ-interactions, our simulations of pentadecane verify that the effect of LJ-PME on homogeneous and isotropic systems is small, and thereby, reparameterization will not be necessary in order for force field parameters in general to be compatible with LJ-PME. However, the same does not necessarily hold for some current lipid force fields directly parametrized to reproduce bilayer properties.

We propose to solve the inherent performance problems when using LJ-PME together with LB combination rules by approximating the dispersion parameters in reciprocal space using geometric combination rules. We have shown that this approximation is sound from a theoretical perspective, that it has limited influence when comparing direct vs reciprocal contributions for a single interaction, and that the errors associated with this assumption are well below the standard deviations of properties obtained from a lipid bilayer simulation

of POPC. This approximation practically solves the computational complexity issues with a performance increase of almost 300% compared to full Lorentz−Berthelot lattice summation. Our current LJ-PME implementation only incurs a performance reduction of roughly 20% compared to twin-range interactions, which we find quite reasonable, and we have good hopes this gap will reduce further with a more optimized implementation in GROMACS that we are currently working on. The fact that nonpolar interactions are of similar sign also means that they exhibit slower fluctuations at large distances, which means it might be possible to only evaluate the reciprocal space component every few steps through the use of a multiple time step algorithm in order to further reduce the cost of the LJ-PME interactions.

Although we have shown that there is no intrinsic need to reparameterize all current force fields in order to use them with LJ-PME, we do believe that more work is needed to improve force fields for future simulations. Lipid bilayer systems are known to be pathologically sensitive to changes in the simulation parameters, such as the electrostatic potential,[5] surface tension[42] and area per lipid.[4] While it might be necessary to revisit some force fields that have been tuned to reproduce bilayer properties if they were developed with truncated LJ-interactions combined with dispersion corrections rather than LJ-PME, there is now great potential for moving beyond the discussion of specific cutoff and interaction schemes and develop lipid force fields that are partly parametrized against properties relevant to lipid bilayers instead of only pure hydrocarbons. These parameters might not be perfect for use in simulation programs that cannot yet use LJ-PME, but even in that case the differences are not expected to be worse than today's imperfect setups, and for the cases where LJ-PME is available, it should provide significantly better accuracy.

With the growing trend of simulations on membrane proteins as well as free energy calculations of both insertion and small molecule interactions, a rigorous method of treating the membrane interactions is of great importance. The force fields commonly used today are often parametrized in order to be used with a specific simulation setup, and if the setup is altered, it might affect the results. There are several examples of sensitivity to setups,[43] not to mention inaccuracies tied to predicting properties that occur over increasingly longer time scales in the future.[44]

The particle mesh Ewald method offers a way of treating long-range interactions without the use of cutoffs but has up until recently only been applied to electrostatic interactions, and it has enabled an accurate treatment of long-range electrostatics without sacrificing too much performance. In many cases, it might be advantageous to move interactions between direct and reciprocal space by altering this cutoff, but the choice of the real space cutoff has been restricted by the Lennard-Jones cutoff in the applied force field. With the introduction of dispersion PME, this restriction is lifted, and it is possible to use direct space cutoffs down to roughly 5 Å, where bonded interactions and the repulsion term start to become important. The ability to treat all long-range interactions using PME should make it possible to develop force fields that are truly independent of specific cutoffs, including those for nonpolar interactions, and achieve more accurate simulations at very little extra cost. The implementation of LJ-PME is planned to be included into the standard version of the GROMACS simulation package in upcoming releases, including further optimizations of the algorithm, and until then, the modified version developed within this work is available as a contributed component at ftp://ftp.gromacs.org/pub/ljpme/.

AUTHOR INFORMATION

Corresponding Author

*E-mail: erik.lindahl@scilifelab.se.

Notes

The authors declare no competing financial interest.

ACKNOWLEDGMENTS

This work was supported by grants from the European Research Council (209825), the Swedish Foundation for Strategic Research, the Swedish Research Council (2010-491, 2010-5107), and the Swedish e-Science Research Center. Computer resources were provided through the Swedish National Infrastructure for Computing (SNIC 020/11-41).

REFERENCES

(1) Hess, B. *J. Chem. Phys.* **2002**, *116*, 209−217.
(2) Hünenberger, P. H.; van Gunsteren, W. F. *J. Chem. Phys.* **1998**, *108*, 6117−6134.
(3) Mark, P.; Nilsson, L. *J. Comput. Chem.* **2002**, *23*, 1211−1219.
(4) Anézo, C.; de Vries, A. H.; Höltje, H.-D.; Tieleman, D. P.; Marrink, S.-J. *J. Phys. Chem. B* **2003**, *107*, 9424−9433.
(5) Patra, M.; Karttunen, M.; Hyvonen, M. T.; Falck, E.; Lindqvist, P.; Vattulainen, I. *Biophys. J.* **2003**, *84*, 3636−3645.
(6) Feller, S. E.; Pastor, R. W.; Rojnuckarin, A.; Bogusz, S.; Brooks, B. R. *J. Phys. Chem.* **1996**, *100*, 17011−17020.
(7) Ewald, P. P. *Ann. Phys.* **1921**, *64*, 253−287.
(8) Hockney, R. W.; Eastwood, J. W. *Computer Simulation Using Particles*; McGraw-Hill: New York, 1981.
(9) Darden, T.; York, D.; Pedersen, L. *J. Chem. Phys.* **1993**, *98*, 10089−10092.
(10) Essmann, U.; Perera, L.; Berkowitz, M. L.; Darden, T.; Lee, H.; Pedersen, L. G. *J. Chem. Phys.* **1995**, *103*, 8577−8592.
(11) Shirts, M. R.; Mobley, D. L.; Chodera, J. D.; Pande, V. S. *J. Phys. Chem. B* **2007**, *111*, 13052−13063.
(12) Klauda, J. B.; Venable, R. M.; Freites, J. A.; O'Connor, J. W.; Tobias, D. J.; Mondragon-Ramirez, C.; Vorobyov, I.; A. D. MacKerell, J.; Pastor, R. W. *J. Phys. Chem. B* **2010**, *114*, 7830−7843.
(13) Ulmschneider, J. P.; Ulmschneider, M. B. *J.Chem. Theory Comput.* **2009**, *5*, 1803−1812.
(14) Venable, R. M.; Chen, L. E.; Pastor, R. W. *J. Phys. Chem. B* **2009**, *113*, 5855−5862.
(15) Lagüe, P.; Pastor, R. W.; Brooks, B. R. *J. Phys. Chem. B* **2004**, *108*, 363−368.
(16) Brooks, B. R.; Brooks, C. L., III; Mackerell, A. D., Jr.; Nilsson, L.; Petrella, R. J.; Roux, B.; Won, Y.; Archontis, G.; Bartels, C.; Boresch, S.; Caflisch, A.; Caves, L.; Cui, Q.; Dinner, A. R.; Feig, M.; Fischer, S.; Gao, J.; Hodoscek, M.; Im, W.; Kuczera, K.; Lazaridis, T.; Ma, J.; Ovchinnikov, V.; Paci, E.; Pastor, R. W.; Post, C. B.; Pu, J. Z.; Schaefer, M.; Tidor, B.; Venable, R. M.; Woodcock, H. L.; Wu, X.; Yang, W.; York, D. M.; Karplus, M. *J. Comput. Chem.* **2009**, *30*, 1545−1614.
(17) Wu, X.; Brooks, B. R. *J. Chem. Phys.* **2005**, *122*, 044107.
(18) Wu, X.; Brooks, B. R. *J. Chem. Phys.* **2008**, *129*, 154115.
(19) Klauda, J. B.; Wu, X.; Pastor, R. W.; Brooks, B. R. *J. Phys. Chem. B* **2007**, *111*, 4393−4400.
(20) Oostenbrink, C.; Villa, A.; Mark, A. E.; Van Gunsteren, W. F. *J. Comput. Chem.* **2004**, *25*, 1656−1676.
(21) Hess, B.; Bekker, H.; Berendsen, H. J. C.; Fraaije, J. G. E. M. *J. Comput. Chem.* **1997**, *18*, 1463−1472.
(22) Berendsen, H. J. C.; Postma, J. P. M.; DiNola, A.; Haak, J. R. *J. Chem. Phys.* **1984**, *81*, 3684−3690.
(23) Parrinello, M.; Rahman, A. *J. Appl. Phys.* **1981**, *52*, 7182−7190.

(24) Berger, O.; Edholm, O.; Jähnig, F. *Biophys. J.* **1997**, *72*, 2002−2013.
(25) Chiu, S.; Pandit, S. A.; Scott, H. L.; Jakobsson, E. *J. Phys. Chem. B* **2009**, *113*, 2748−2763.
(26) Berendsen, H. J. C.; Grigera, J. R.; Straatsma, T. P. *J. Phys. Chem.* **1987**, *91*, 6269−6271.
(27) Berendsen, H. J. C.; Postma, J. P. M.; van Gunsteren, W. F.; Hermans, J. In *Intermolecular Forces*; Pullman, B., Ed.; D. Reidel Publishing Company: Dordrecht, 1981; pp 331−342.
(28) Hub, J. S.; Winkler, F. K.; Merrick, M.; de Groot, B. L. *J. Am. Chem. Soc.* **2010**, *132*, 13251−13263.
(29) Jorgensen, W. L.; Tirado-Rives, J. *J. Am. Chem. Soc.* **1988**, *110*, 1657−1666.
(30) Kumar, S.; Bouzida, D.; Swendsen, R. H.; Kollman, P. A.; Rosenberg, J. M. *J. Comput. Chem.* **1992**, *13*, 1011−1021.
(31) Hub, J. S.; de Groot, B. L.; van der Spoel, D. *J. Chem. Theor. Comput.* **2010**, *6*, 3713−3720.
(32) Horn, H. W.; Swope, W. C.; Pitera, J. W.; Madura, J. D.; Dick, T. J.; Hura, G. L.; Head-Gordon, T. *J. Chem. Phys.* **2004**, *120*, 9665−9678.
(33) Jorgensen, W. L.; Maxwell, D. S.; Tirado-Rives, J. *J. Am. Chem. Soc.* **1996**, *118*, 11225−11236.
(34) Dovnar, D.; Lebedinskii, Y.; Khasanshin, T.; Shchemelev, A. *High Temp.* **2001**, *39*, 835−839.
(35) Somerharju, P.; Virtanen, J.; Eklund, K.; Vainio, P.; Kinnunen, P. *Biochem.* **1985**, *24*, 2773−2781.
(36) Kucerka, N.; Tristram-Nagle, S.; Nagle, J. F. *J. Membr. Biol.* **2005**, *208*, 193−202.
(37) Kucerka, N.; Nagle, J. F.; Sachs, J. N.; Feller, S. E.; Pencer, J.; Jackson, A.; Katsaras, J. *Biophys. J.* **2008**, *95*, 2356−2367.
(38) Seelig, J.; Waespe-Sarcevic, N. *Biochemistry* **1978**, *17*, 3310−3315.
(39) Douliez, J.-P.; Léonard, A.; Dufourc, E. J. *Biophys. J.* **1995**, *68*, 1727−1739.
(40) Egberts, E.; Marrink, S. J.; Berendsen, H. J. C. *Eur. Biophys. J.* **1994**, *22*, 423−436.
(41) Klauda, J. B.; Brooks, B. R.; MacKerell, A. D., Jr.; Venable, R. M.; Richard; Pastor, W. *J. Phys. Chem. B.* **2005**, *109*, 5300−5311.
(42) Feller, S. E.; Pastor, R. W. *J. Chem. Phys.* **1999**, *111*, 1281−1287.
(43) Piggot, T. J.; ÁngelPi, neiro; Khalid, S. *J. Chem. Theory Comput.* **2012**, *8*, 4593−4609.
(44) Freddolino, P. L.; Liu, F.; Gruebele, M.; Schulten, K. *Biophys. J.* **2008**, *94*, L75−L77.